Tuning of quantum entanglement in molecular quantum cellular automata based on mixed-valence tetrameric units

Andrew Palii,[1,2*] Boris Tsukerblat [3*]

[1]*Institute of Problems of Chemical Physics, Russian Academy of Sciences,*

Chernogolovka, Moscow Region, Russia

[2]*Institute of Applied Physics, Academy of Sciences of Moldova, Kishinev, Moldova*

[2]*Ben-Gurion University of the Negev, Beer-Sheva, Israel*

[*]E-mail: andrew.palii@uv.es (A.P.), tsuker@bgu.ac.il (B.T.)

Abstract

In this article we consider two coupled tetrameric mixed-valence (MV) units accommodating electronic pairs which play role of cells in molecular quantum cellular automata. It is supposed that the Coulomb interaction between instantly localized electrons within the cell markedly inhibits the transfer processes between the redox centers. Under this condition, as well as due to the vibronic localization of the electronic pair, the cell can encode the binary information which is controlled by the neighboring cells. We show that under certain conditions the two low lying vibronic spin levels of the cell (ground and first excited) can be regarded as originating from an effective spin-spin interaction. The last is shown to depend on the internal parameters of the cell as well as on the induced polarization. Within this simplified two-level picture we evaluate the quantum entanglement in the system represented by the two electrons in the cell and show how the entanglement within the cell and concurrence can be controlled via polarization of the neighboring cell and temperature.

1. Introduction

Entanglement is one of the fundamental and most intriguing phenomenon lying in core of the quantum-mechanical description of the matter (see books [1, 2]). Quantum entanglement is now in focus of a wide area of research dealing with the applications in quantum computing, cryptography, communication, teleportation and related issues [3-5]. The main effects of entanglement have been detected experimentally with photons [6, 7], electrons and molecules [8]. Recently, the problem of entanglement became a fascinating part of a

wide area of molecular magnetism [9-12] since the magnetic clusters have been proposed as novel objects for spin-based implementation of quantum-information processing [13-20].

Engineering the coupling between molecular spin qubits by coordination chemistry have been thoroughly discussed in Ref. [21, 22] with the emphasis on antiferromagnetic Cr_7Ni rings ($[NH_2Pr_2][Cr_7NiF_8(O_2CCMe_3)_{16}]$ and $[NH_2Pr_2][Cr_7NiF_8(O_2CCMe_3)_{15}(O_2CC_5H_4N)]$) which behave as effective spin-1/2 systems. In particular, $Cr_7Ni–Cu–Cr_7Ni$ fragment can be represented as a system for investigating tripartite entanglement in molecular spin qubits for which the numerical simulation of entangled states has been performed [21,22]. Spin triangles as optimal units for molecule-based quantum gates have been proposed in Ref. [18]. The latest achievements in this area was marked by the design of molecular prototypes for spin-based CNOT and SWAP quantum gates [23], chemical engineering of heterodimetallic lanthanide complexes mimicking two-qubit molecular spin quantum gates [24], modular design of molecular qubits [25].

Quantum entanglement in binuclear nitrosyl iron complexes $[Fe_2(C_3H_3N_2S)_2(NO)_4]$ and $[Fe_2(SC_3H_5N_2)_2(NO)_4]$ has been considered in Ref. [20] where the temperature dependence of entanglement has been expressed in terms of the magnetic susceptibility for a Heisenberg dimer. Observation of room-temperature entanglement between single defect spins in diamond was an important step towards the development of quantum information technologies [26]. The concepts of quantum entanglement and quantum discord in different materials with ferro- and antiferromagnetic coupling have been reviewed in Ref. [27] along with the examples demonstrating the presence of non-local quantum correlations.

Development in the field of quantum computing have been strongly impacted by the paradigm of quantum-dot cellular automata (QCA) [28], a scheme for molecular electronics in which information is transmitted and processed through electrostatic interactions in an array of cells [28-31]. The semiconductor- (or metal) based QCA have been realized as dots
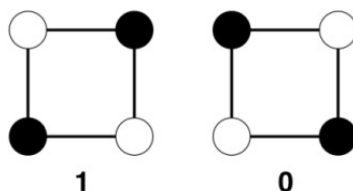
Figure 1. Two charge distributions encoding binary **1** and **0** in a four-dot QCA cell or in a molecular QCA cell composed of four redox centers in a square mixed-valence molecule. Black balls-dots or redox centers accommodating electrons, white balls-"empty" dots (redox centers).

composing wires and majority gates on a silicon substrate . The binary information (**1** and **0**) is encoded in the two antipodal charge configurations of a four-dot cell (Fig. 1) and can be transmitted via Coulomb interaction between the neighboring cells. The complex circuits are built as grids of the logical gates such as majority gates, fun-out, invertors, wires, etc. [28-30].

More recently the promising idea to use the molecules instead of dots has been proposed and thoroughly discussed [31-33]. Molecular QCA are expected to result in further miniaturization of microelectronic devices and in a substantial increase of their advantages, such as ultra-high device densities and room-temperature operation. As a single molecule implementation of QCA it has been proposed to use 1,4-dialyl butane radical cation consisting of butyl bridge linking the two allyl groups accommodating the electrons [34]. Then, the problem of molecular QCA and other attractive candidates for molecular cells have been proposed and discussed in detail in Refs. [35-44]. Examples include mixed-valence (MV) complex $[\{(\eta^5\text{-}C_5H_5)Fe(\eta^5\text{-}C_5H_4)\}_4(\eta^4\text{-}C_4)Co(\eta^5\text{-}C_5H_5)]^{2+}$ [38] as well as tetra-ruthenium 2Ru(II)+2Ru(III) complexes assembled as two coupled Creutz-Taube dimers in the center-bridged and side-bridged square-planar tetramers [45].

Since MV cell for molecular QCA contains two electrons (or holes) delocalized over four metal sites it would be interesting to find out whether these two electrons (two state systems like two qubits) can be entangled. In the present article we develop a vibronic model which adequately describes the low lying energy pattern of the cell and takes into account the cell-cell interaction. We show that under certain conditions implied by interrelation between the electron transfer parameters, vibronic coupling and Coulomb repulsion between itinerant electrons the energy pattern of the cell involves well isolated spin- singlet and spin-triplet vibronic levels. This is shown to be just a necessary condition for an effective spin coupling similar to that observed in spin-dimers for which the existence of quantum entanglement was demonstrated [20]. We consider quantum entanglement in the tetrameric MV cell ("output cell") coupled to the neighboring cell ("input cell") having a certain polarization associated with a particular distribution of the electronic density. In this way one can reveal the temperature dependence of quantum entanglement in "output" cell calculated at different polarizations of the "input" cell as well as the critical temperature (below which quantum entanglement can exist) as function of the cell parameters. It is demonstrated a possibility of tuning of quantum entanglement in molecular QCA based on mixed-valence tetrameric units via proper polarization of the "input" cell.

2. Vibronic model of polarized mixed valence two-electron square cell

The vibronic model of a MV square planar cell has been developed in our recent papers [46, 47]. Hereafter we will only briefly describe the key interactions involved in the model with emphasis on aims of the present consideration. There are three key interactions which act in an isolated MV cell, namely, the electrostatic interaction between the electrons, electron transfer and vibronic interaction. Conventionally, the electron transfer facilitates the delocalization between the redox centers, while the vibronic coupling is responsible for the self-trapping, competing thus with the electron transfer. The Coulomb repulsion plays a special role distributing the electron density on the most remote sites which is specially important for the encoding of information. Thus, the interactions so far mentioned have distinct key physical meanings and, hence, they are inherent in MV system, although their specific manifestations depend on the topology and electronic structure of the system. Although the number of the parameters within the semiempirical approach is rather large they should be taken into account for the physically justified description of the MV cell. Hopefully, the microscopic analysis together with the analysis of experimental data can shed light on the real interrelation between these parameters.

As usually, we will first consider the energy pattern of the system providing that the position of the ions of the cell are fixed (electronic problem) and then the interaction of the electrons with the molecular vibrations will be taken into account.

2.1. *Electronic interactions within the cell.* The main electronic intracell interactions and corresponding parameters are schematically shown in Fig. 2. There are six possibilities to distribute two extra electrons between four sites. Two of these distributions correspond to the localization of the two electrons in the distant (d) antipodal positions (along the diagonals of the square), while the remaining four distributions are those in which the two itinerant electrons are localized at the nearest neighboring (n) sites (along the edges of the square cell). The interelectronic Coulomb repulsion energies U_d and U_n for the electronic distributions of d and n-types are different with $U_n > U_d$ because the Coulomb repulsion tends to keep the two itinerant electrons as far as possible. Thus the d and n-type distributions form the ground and excited Coulomb multiplets of the cell, respectively. The only intracell Coulombic parameter that is important here is the energy gap $U = U_n - U_d$ between these two Coulomb multiplets (Fig. 2a).
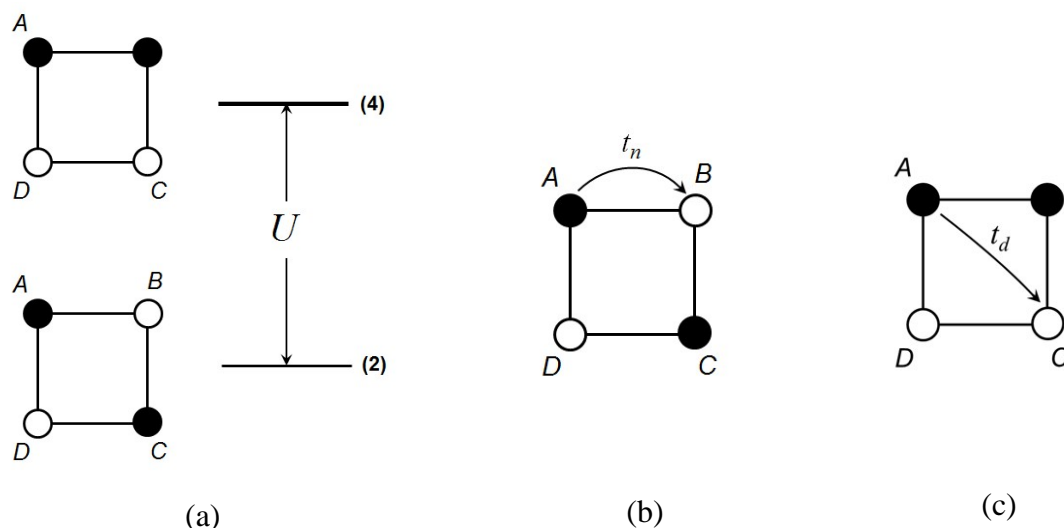
Figure 2. Illustration of the key electronic interactions in the square-planar MV molecular QCA cell with two extra electrons: (a) Coulomb gap between n and d – multiplets, where the numbers in the parentheses are the multiplicities (numbers of the electronic distributions); (b) electron transfer along the edge of the cell; (c) electron transfer along the diagonal of the cell.

Then we assume that electrons can jump from the occupied site to the empty one within the cell. This one-electron hopping can occur along the edge (Fig. 2b) or along the diagonal (Fig. 2c) of the square cell, with corresponding electron transfer parameters being denoted as t_n and t_d respectively. These transfer integrals are quite similar to those involved in Hubbard-type Hamiltonians widely used in solid state physics. The physical roles of the t_n and t_d transfer processes are quite different. The jumps of the t_n type transform a certain antipodal charge configuration into a neighboring one (Fig.2b), while t_d transfer switches between two different n- configurations (Fig. 2c). The interrelation between these parameters is crucially dependent of the topology of the system which in its turn determines the network of the efficient transfer pathways. Relevant examples of the two types of MV tetra-ruthenium complexes are given in Refs. [46, 47] , where one can find references on the original papers about these compounds.

The electronic wave-functions corresponding to a definite localization of the electronic pair and spin S of the electronic pair can be expressed in terms of the bi-electronic Slater determinants as follows:

$$\psi_{ij}(S=0) = \frac{1}{\sqrt{2}}\left(\left|\varphi_i\bar{\varphi}_j\right| - \left|\bar{\varphi}_i\varphi_j\right|\right), \qquad \psi_{ij}(S=1, M_S=1) = \left|\varphi_i\varphi_j\right|, \tag{1}$$

where only spin-triplet wave-function with maximal spin projection is given. The set of indices $\{i, j\}$ run over the sites A, B, C and D, φ and $\bar{\varphi}$ are the spin-orbitals with "spin-up" and "spin-down", correspondingly. The distant pairs $\{A, C\}$ and $\{B, D\}$ relate to the states belonging to the ground Coulomb manifold, while the neighboring pairs $\{A, B\}$, $\{B, C\}$, $\{C, D\}$, and $\{A, D\}$ are those for the excited manifold. It is easy to imagine that any one-electron transfer process occurring within the ground manifold results in the Coulombic excitation of the two-electron MV square. Hence the one-electron transfer processes t_n and t_d can transform the two ground states $\psi_{AC}(S)$, $\psi_{BD}(S)$ (with the same spin S) into each other only through several steps via the states belonging to the excited manifold. We will assume here that the intra-site Coulomb energy U significantly exceeds the transfer parameters t_n and t_d. Otherwise the transfer processes would not be able to localize the electrons at the antipodal positions so that the cell could store information. We referred this most relevant case to as "strong U-approximation" [46,47] for which the perturbation theory (with the smallness parameters $|t_n|/U$, $|t_d|/U$) is applicable. Since we are interested to deal with the low lying levels it is reasonable to obtain the effective Hamiltonian acting in the reduced subspace of ground Coulomb manifold composed of the wave-function of the d-pairs. As usually, the effective Hamiltonian can be deduced with the use of the projection operator. For example, in the case under consideration within which all unperturbed energies are equal to U, the second order term can be expressed as:

$$\mathbf{H}_{eff} = \frac{1}{U} \sum_{\lambda} \mathbf{H} |\lambda\rangle\langle\lambda| \mathbf{H}, \tag{1}$$

where $\mathbf{H}$ is the exact Hubbard Hamiltonian which take into account all transfer processes (Eq. (2) in Ref. [46]) and the summation is performed over excited states $|\lambda\rangle$. In this way one can obtain the following matrix representation of the electronic Hamiltonian of the cell projected onto the space of d-states. The blocks with $S = 0$ and $S = 1$ defined in the basis $\psi_{AC}(S)$, $\psi_{BD}(S)$ are the following:

$$\mathbf{H}_c(S=0) = -\frac{4t_n^2}{U}\left(1 - 2\frac{t_d}{U}\right)(\mathbf{1}_e + \boldsymbol{\sigma}_Z), \quad \mathbf{H}_c(S=1) = -\frac{4t_n^2}{U}\mathbf{1}_e, \tag{2}$$

where $\boldsymbol{\sigma}_Z$ is the Pauli matrix, $\mathbf{1}_e$ is the unit 2×2- matrix, and the nonvanishing terms in the perturbation series (up to the third order terms, which are proportional to t_n^2/U and $t_n^2 t_d/U$) are retained. It is to be noted that the transfer parameter t_d does not contribute to

the spin triplet states, while in spin singlet states it appears in the third order of perturbation theory. The contributions of t_n appears in both spin-triplet (second order contribution) and spin-singlet (second-order and third-order contributions) states. The Hamiltonian, Eq.(2),
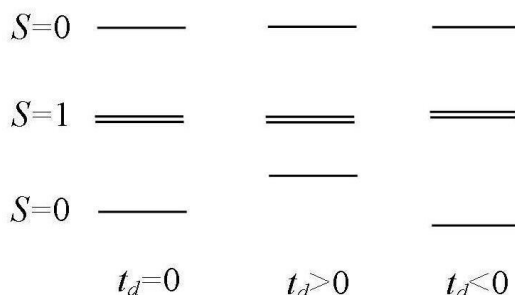
Figure 3. Scheme of the low lying levels of the tetrameric MV cell illustrating the role of the transfer parameter t_d.

describes the low-lying part of the electronic energy pattern of the MV cell that (as follows from Eq. (2)) consists of the double degenerate spin-triplet with the energy $-4t_n^2/U$ and two spin-singlets having the energies 0 and $-\left(8t_n^2/U\right)\left(1-2t_d/U\right)$ as schematically shown in Fig. 3 for the cases $t_d = 0$, $t_d > 0$ and $t_d < 0$. One can see that the positions of the levels are independent of the sign of t_n, while the sign of t_d affects the position of the ground level as shown in Fig. 3.

One can see a significant difference between the spin-triplet and spin-singlet states, namely, for $S = 1$ the off-diagonal matrix elements connecting the states $\psi_{AC}(S=1)$ and $\psi_{BD}(S=1)$ are zero, while for $S = 0$ such matrix element is nonvanishing and contains both second and third order contributions. On the contrary, the electron transfer (t_n) contributes only to the diagonal matrix elements in the $\mathbf{H}_c(S=1)$-block. This second order contribution corresponds to the two-step electron transfer process in course of which the electron jumps with the excitation U to the neighboring site (first step) and then jumps back to the initial site restoring the ground manifold (second step). It is important to note that difference between the states with $S = 1$ and $S = 0$ is of crucial importance for our consideration, because it means that the cells in spin singlet and spin triplet states possess different polarizabilities under the action of quadrupole electric field induced by the neighboring cell. In fact it is more

easy to polarize the cell in $S = 1$ state because of the absence of extra-diagonal resonance matrix elements promoting electron delocalization.

2.2. *Cell-cell coupling.* Now let us consider the Coulomb interaction of cell **1** with the neighboring cell **2** having a definite polarization P_2. The polarization of a cell can be characterized by a scalar quantity P [31] which can be regarded as a normalized measure of the degree to which the electron densities are localized in antipodal positions along the diagonals (*AC* or *BD*, Fig. 3) of a square planar four-dot cell. According to this definition the value P_2 can be written as

$$P_2 = \frac{(\rho_A + \rho_C) - (\rho_B + \rho_D)}{\rho_A + \rho_B + \rho_C + \rho_D}, \tag{3}$$

where ρ_i is the electronic density on the site i. Since we are dealing with the polarization relating to the ground (distant pairs) distributions of the electronic density, one can put $\rho_A = \rho_C = \rho$ and $\rho_B = \rho_D = 1 - \rho$ $(0 \leq \rho \leq 1)$ and, therefore, $P_2 = 2\rho - 1$ or $\rho = (1 + P_2)/2$. Providing $\rho = 0$ and 1 the cell **2** is fully polarized along the diagonals, the corresponding polarizations take on the values -1 and +1. It was shown [47], that the Hamiltonian of the cell **1** polarized by the quadrupole Coulombic field created by the cell **2** prepared in a certain polarization P_2 can be presented in the following matrix form in the $\psi_{AC}(S)$, $\psi_{BD}(S)$-basis:

$$\mathbf{H}_{c-c} = \frac{1}{2} u \, \boldsymbol{\sigma}_z \,. \tag{4}$$

In this expression $u = (U_{AC} - U_{BD})/2$, where U_{AC} and U_{BD} are the energies of the Coulomb repulsion between the cell **1**, in which the two extra electrons are localized along the diagonals AC and BD, respectively, and the polarized cell **2** possessing some definite arbitrary polarization P_2. As it follows from this definition the value u depends on P_2 as well as on the geometrical parameters of the system. To find this dependence we consider the charge distributions corresponding to the Coulomb energies U_{AC} and U_{BD} which are shown in Figs. 4a and 4b. Then one can derive the parameter u in terms of polarization P_2 and intra- and intercell distances b and c (Fig. 2) as follows:

$$u = P_2 e^2 \left[\frac{1}{b+c} + \frac{1}{2\sqrt{(2b+c)^2 + b^2}} + \frac{1}{2\sqrt{b^2 + c^2}} - \frac{1}{\sqrt{(b+c)^2 + b^2}} - \frac{1}{2(2b+c)} - \frac{1}{2c} \right]. \tag{5}$$

It is to be noted that the parameter u is proportional to the polarization P_2.

(a)

(b)
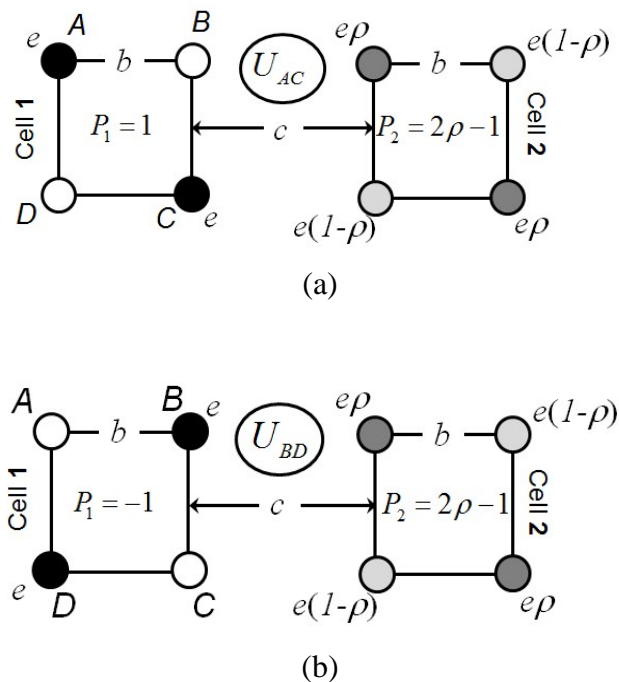
Figure 4. Charge distributions corresponding to the Coulomb energies U_{AC} (a) and

U_{BD} (b).

The quadrupole Coulombic field of the cell **2** lowers the symmetry of the cell **1** and splits the orbitally degenerate spin triplet into two levels with the energies $-4t_n^2/U \pm u$ and mixes the two spin singlets giving rise to the energies

$$-\frac{4t_n^2}{U}\left(1-2\frac{t_d}{U}\right)\pm\left[\frac{u^2}{4}+\frac{16t_n^2}{U}\left(1-2\frac{t_d}{U}\right)\right]^{1/2}.$$

One can see that the Coulomb forces stabilize spin-singlet and spin-triplet levels, the last stabilization proves to be more strong. It should be noted that at a definite value of u the $S=0$ and $S=1$ levels cross.

2.3. *Vibronic coupling.* An important ingredient of the model of MV cell is the vibronic coupling which strongly influences the degree of electron localization by producing the so-called self-trapping effect. The model for the vibronic coupling in molecular QCA based on MV square planar cells was developed in our recent articles [46,47]. We have demonstrated that within the strong U limit the bi-electronic formation of the cell is coupled to the only vibrational mode Q in the Piepho, Krausz and Schatz (PKS) model [48] conventionally used when describing the MV compounds. The "out-of-phase" vibrational

mode Q (having B_{1g} symmetry in the point group $\mathbf{D}_{4h}$) can be imagined as expansion of the first ligand coordination spheres for two antipodal sites (say, A and B) accompanied by simultaneous compression of the coordination spheres for other pair of antipodal sites (C and D) or vice versa as shown in Fig. 5).
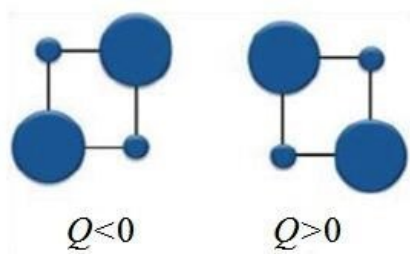
Figure 5. Schematic representation of the atomic displacements in the active mode Q of a square-planar cell.

The matrix of the vibronic Hamiltonian in the basis $\psi_{AC}(S)$, $\psi_{BD}(S)$ is given by [47]:

$$\mathbf{H}_{vib} = -\upsilon Q \boldsymbol{\sigma}_z, \tag{6}$$

where Q is the dimensionless vibrational coordinate and υ is the vibronic coupling parameter defined as usually in PKS model for MV compounds. In particular case of a tetrameric system this definition is given in Ref.[7] (for the sake of brevity we will not repeat it here). In the case of spin singlets (first formula in Eq. (2)) the interaction with this vibration results in the pseudo Jahn-Teller effect. Finally, one has to take into account also the Hamiltonian

$$\mathbf{H}_Q = \frac{\hbar\omega}{2}\left(Q^2 - \frac{\partial^2}{\partial Q^2}\right)\mathbf{1}_e \tag{7}$$

describing the free harmonic oscillations with the frequency ω associated with the Q-mode. Then with allowance of all above described interactions the S- block of the matrix of the full Hamiltonian includes electronic Hamiltonian of a cell, Coulomb field of the neighboring cell, free vibrations of the cell and vibronic coupling:

$$\mathbf{H}(S) = \mathbf{H}_c(S) + \mathbf{H}_{c-c} + \mathbf{H}_{vib} + \mathbf{H}_Q. \tag{8}$$

This Hamiltonian represents a matrix in the electronic space $\psi_{AC}(S)$, $\psi_{BD}(S)$, were the functions $\psi_{AC}(S)$, $\psi_{BD}(S)$ are the bi-electronic Slater determinants composed of the

orbitals localized on the sites *A,C* and *B,D* correspondingly and adapted to *S*=1 and *S*=0 spin symmetry.

3. Vibronic energy pattern of a polarized mixed valence cell

Numerical diagonalization of the Hamiltonian gives the spin-vibronic energy pattern of the cell. The two electronic states with $S = 1$ are not mixed by the Q-mode and therefore one can apply the shift transformation to the coordinate Q and to pass from the basis $\psi_{AC}(S=1)\chi_n(Q)$, $\psi_{BD}(S=1)\chi_n(Q)$ to the basis

$$\psi_{AC}(S=1)\chi_n\left(Q-\frac{\upsilon}{\hbar\omega}\right), \qquad \psi_{BD}(S=1)\chi_n\left(Q+\frac{\upsilon}{\hbar\omega}\right) .$$

In this basis the equilibrium positions of the harmonic oscillators are shifted to the adiabatic potential minima. The matrix $\mathbf{H}_{tot}(S=1)$ proves to be diagonal and one immediately obtains for the spin-vibronic levels with *S*=1 the energies $-4t_n^2/U \pm u + \hbar\omega(n+1/2)$.

In case of spin-singlets no analytical solution is available and one has to solve the dynamic pseudo-Jahn-Teller vibronic problem. In the numerical diagonalization of the matrix $\mathbf{H}_{tot}(S=0)$ we have taken 200 vibrational levels (n_{max}=199) that is quite enough to reproduce the lowest spin-vibronic energy levels with a good accuracy.

The energy levels $\varepsilon_v(S)$ and corresponding vibronic wave-functions $\psi_v(S)$ (v=1, 2…) obtained in this way give information about the cell. Particularly, the knowledge of the wave-functions of the cell makes it possible to evaluate the distribution of the electronic density within the cell and its polarization. By considering the cell in the Coulombic field created by the neighboring cell one can find the polarization P_1 as function of polarization P_2 of the neighboring cell. This is the so the called cell-cell response function that is one of the key characteristic determining the functionality of molecular QCA. The cell-cell response function in molecular QCA based on the vibronic model of MV cells was discussed in Ref. [47]. Here we will focus on the quantum entanglement in the cell **1** and its dependence on the polarization of the cell **2**.

The typical patterns of the spin-vibronic energy levels of the cell **1** calculated as functions of the polarization P_2 of the neighboring cell are shown in Fig. 6. We use for the vibronic coupling parameter and vibrational quanta the values $\upsilon = 200\,\text{cm}^{-1}$ and $\hbar\omega = 300\,\text{cm}^{-1}$, which are in the range of typical values of these parameters. The intra-cell distance is taken to be $b = 3.5\,\overset{\text{o}}{\text{A}}$ (within the range of typical intra-cluster metal-metal

distances in molecular magnetic clusters [10, 11]), while the used inter-cell distance $c = 6 \overset{\circ}{A}$ it taken to assure an efficient influence of the neighboring cell **2** on the properties of the cell **1**. The last distance is close to that used in Ref. [32] as a distance between the driver and output cell in molecular QCA. To estimate the order of magnitude of the parameter $4t_n^2/U$ one can assume that a typical value of U is 10,000 cm^{-1} while for MV metal clusters the transfer parameter can be approximately 1000 cm^{-1} and therefore $4t_n^2/U \approx 100\,cm^{-1}$. This value preserves the conditions under which the perturbation scheme (strong $U-$ limit) works properly.

Depending on the parameter t_d one can distinguish two types of the energy patterns which are shown in Figs. 6a and 6b. Thus, when $t_d/U = 0.075$ (Fig. 6a) and providing P_2=0 the ground level is spin-singlet. Polarization of cell **2** ($P_2 \neq 0$) induces the polarization of the cell **1** and, thus, gives rise to the stabilization of both lowest spin singlet and spin triplet

(a)   (b)
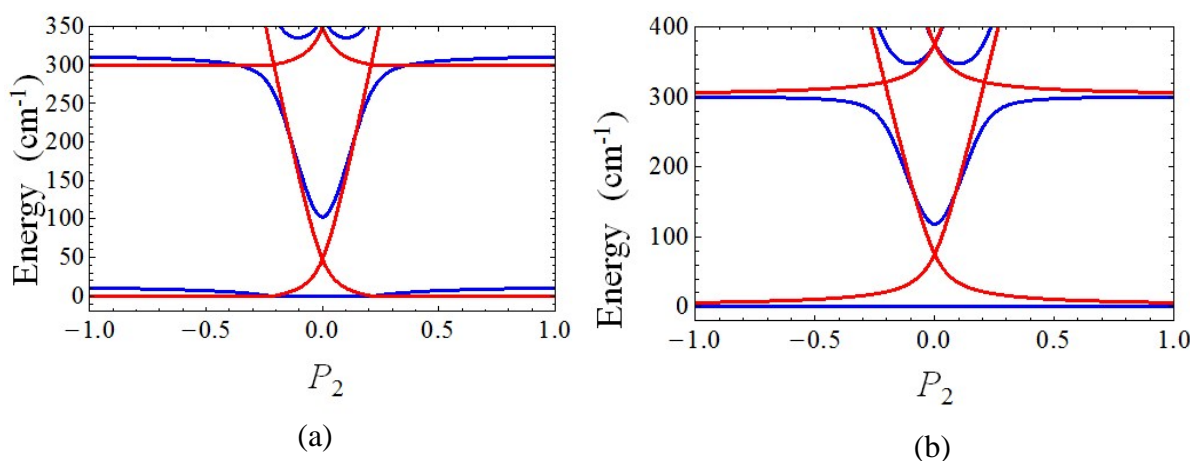
Figure 6. Low-lying vibronic energy levels of cell **1** calculated as a function of the

polarization P_2 of cell **2** with $4t_n^2/U = 100\,cm^{-1}$, $\hbar\omega = 300\,cm^{-1}$, $\upsilon = 200\,cm^{-1}$,

$b = 3.5 \overset{\circ}{A}$, $c = 6 \overset{\circ}{A}$ and $t_d/U = 0.075$ (a) or $t_d/U = 0$ (b). Coloring: $S = 1$ - red

lines, $S = 0$ - blue lines; the energy of the ground state is chosen as the reference

level.

levels. One can see that the triplet is stabilized stronger and so the increase of P_2 leads to the decrease of the energy gap $J = \varepsilon_1(S = 1) - \varepsilon_1(S = 0)$ between the lowest vibronic spin singlet and spin triplet. Finally, at some critical value of P_2 these levels cross and the spin triplet

becomes the ground state which means that the energy gap J at this point becomes negative. On the contrary, for the case of $t_d/U = 0$ shown in Fig. 3b (the diagonal electron transfer is vanishing, for instance, due to the absence of the bridge mediating this transfer) the cell-cell interaction does not lead to the crossing of the levels with $S = 0$ and $S = 1$ even at maximally polarized cell 2 ($|P_2|=1$) although the energy gap in this case is strongly reduced.

3. Quantum entanglement in a polarized cell

A remarkable feature of the energy patterns in Fig. 6 is that in both cases for large enough values of polarization $|P_2|$ (roughly, larger than 0.1) the low-lying part of the energy spectra comprises two isolated levels (spin singlet and spin triplet), while the rest of the spin-vibronic levels are significantly higher in energy. This low-lying part of the energy pattern can be thus regarded as a result of an effective exchange coupling of the electronic spins in the cell. This coupling can be described by the effective Heisenberg-Dirac-Van Vleck exchange Hamiltonian of the form

$$\mathbf{H}_{eff} = -2J \, \mathbf{s}_1 \mathbf{s}_2 \ , \tag{10}$$

in which $s_1 = s_2 = 1/2$ and J is just the above described energy gap between the lowest spin-singlet and spin-triplet levels. The dependences of the parameter J on the polarization P_2 calculated for the two above considered cases are shown in Fig. 7. It is seen from Fig. 3a

(a)   (b)
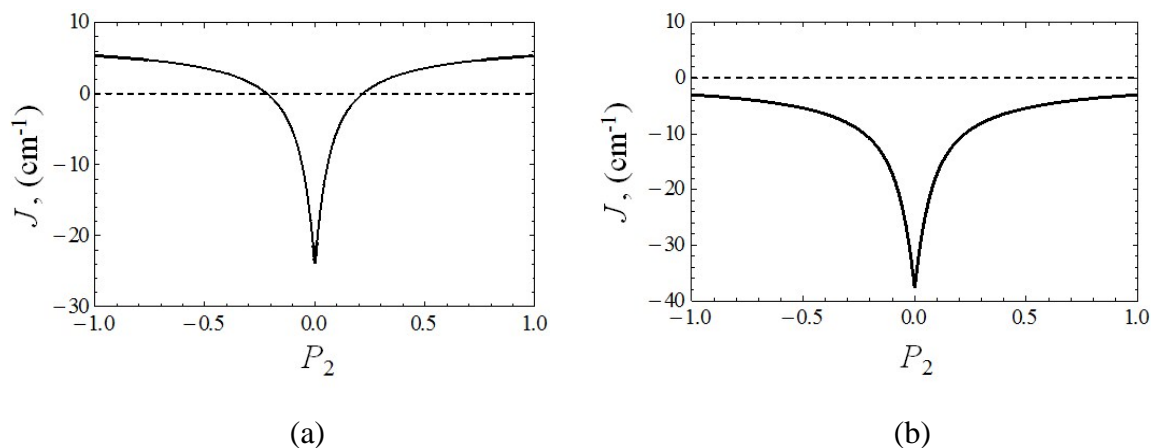
Figure 7. Effective exchange parameter for cell **1** calculated as function of polarization P_2 with the same sets of parameters as in Fig. 6a and 6b.

that for $t_d/U = 0.075$ the exchange coupling is antiferromagnetic ($J < 0$) in the weak polarization region, while for $|P_2|$ above some critical value (≈ 0.21) this interaction becomes

ferromagnetic. In case $t_d/U = 0$ (Fig. 7b) variation of the polarization P_2 cannot change the sign of the exchange parameter which remains always negative. At the same time polarization tends to suppress the antiferromagnetic coupling between the spins and therefore in both cases the inter-cell interaction produces ferromagnetic effect.

The above introduced approximate two-level picture based on the effective exchange Hamiltonian, Eq. (10), allows us to significantly simplify the evaluation of quantum entanglement. For the two-qubit systems (bi-spin system in the case under consideration) the entanglement of formation is related to the concurrence C as follows [1]:

$$E = h\left[\frac{1}{2}\left(1 + \sqrt{1 - C^2}\right)\right]. \tag{11}$$

In Eq. (11) the function $h(x)$ is the von Neumann entropy for a binary probability distribution:

$$h(x) = -x\,log_2(x) - (1 - x)\,log_2(1 - x). \tag{12}$$

The concurrence depends on the density matrix of the system. Under the condition of thermal equilibrium the density matrix for a Heisenberg dimer with spins 1/2 (Bleaney–Bowers dimer) that is described by the exchange Hamiltonian, Eq. (10), has the following form:

$$\boldsymbol{\rho}(T) = \frac{1}{Z}\exp\left(-\frac{\mathbf{H}_{eff}}{k_B T}\right) = \begin{pmatrix} v & 0 & 0 & 0 \\ 0 & p & w & 0 \\ 0 & w & p & 0 \\ 0 & 0 & 0 & v \end{pmatrix}, \tag{13}$$

where the basis $\left|\uparrow\uparrow\right\rangle$, $\left|\uparrow\downarrow\right\rangle$, $\left|\downarrow\uparrow\right\rangle$, and $\left|\downarrow\downarrow\right\rangle$ is used. Here the value

$$Z = 3\exp\left(\frac{J}{2k_B T}\right) + \exp\left(-\frac{3J}{2k_B T}\right) \tag{14}$$

is the partition function. In Eq. (14) the following notations are used:

$$v = \frac{1}{Z}\exp\left(\frac{J}{2k_B T}\right),$$
$$p = \frac{1}{Z}\exp\left(-\frac{J}{2k_B T}\right)\cosh\left(\frac{J}{k_B T}\right), \tag{15}$$
$$w = \frac{1}{Z}\exp\left(-\frac{J}{2k_B T}\right)\sinh\left(\frac{J}{k_B T}\right).$$

One can prove [20] that in this particular case the concurrence can be calculated with the aid of the expression

$$C = 2\max\left\{|w| - v,\ 0\right\},\tag{16}$$

that is the particular case of well-known Wootters formula for bipartite (two-qubit) entanglement [49,50]. It directly follows from Eqs. (15) and (16) that in the case of ferromagnetic exchange one finds that $C = 0$ at all temperatures and hence, according to Eq. (11), no entanglement can exist in this case. Providing antiferromagnetic exchange one obtains from Eqs. (15) and (16) the following expression for the concurrence [20]:

$$C(T) = \frac{1 - 3\exp\left(-\dfrac{2|J|}{k_B T}\right)}{1 + 3\exp\left(-\dfrac{2|J|}{k_B T}\right)},\quad T < T_E,\tag{17}$$

$$C(T) = 0,\quad T \geq T_E,$$

From. Eq. (17) one can see that the value

$$T_E = \frac{2|J|}{k_B \ln(3)}.\tag{18}$$

is the critical temperature above which the entanglement disappears.

Figure 5 presents the temperature dependence of quantum entanglement evaluated at different values of P_2 with the aid of Eqs. (11), (17) and with the use of the calculated dependences $J\ (P_2)$ (Figure 7). Providing $t_d/U = 0.075$ (Figure 5a) and weak polarization

(a)

(b)
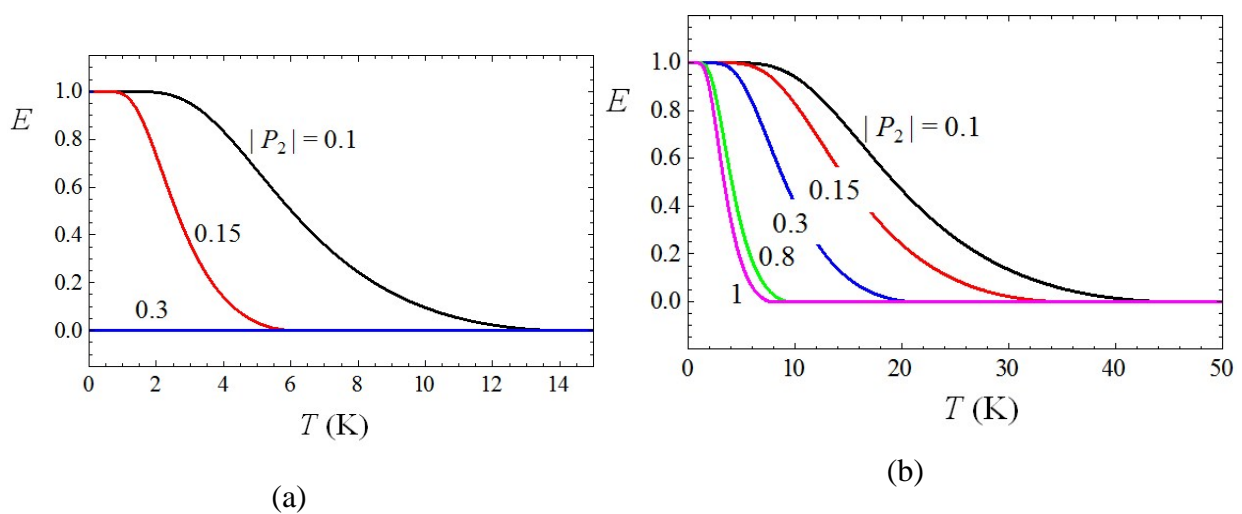
Figure 8. Temperature dependences of quantum entanglement in cell **1** calculated at different polarizations P_2 with the same sets of parameters as in Fig. 6 a and 6b.

$|P_2|$=0.1 the system is fully entangled ($E = 1$) in the low-temperature limit when only the spin-singlet state is thermally populated. Then, with the increase of the temperature the value of E decreases and disappears at approximately $T_E \approx 13.5\,\mathrm{K}$. Providing stronger polarization (case of $|P_2|$=0.15 in Fig. 8a) the temperature at which entanglement disappears is lower $(T_E \approx 6\mathrm{K})$. Finally, providing strong enough polarization (case of $|P_2|$=0.3 in Fig. 8a) no entanglement exists even at zero temperature. This is evidently because of the fact that at such polarization the effective exchange coupling is ferromagnetic and the ground state is spin-triplet level which corresponds to unentangled states. In contrast, providing $t_d/U = 0.075$ (Fig. 8b) the system proves to be entangled in the low-temperature limit even for maximal polarization $|P_2|$=1, but the critical temperature T_E in this case is strongly reduced (from around 44 K for $|P_2|$=0.1 to around 9K for $|P_2|$=1). In general, one can see that the increase of polarization of the neighboring cell tends to destroy the quantum entanglement.
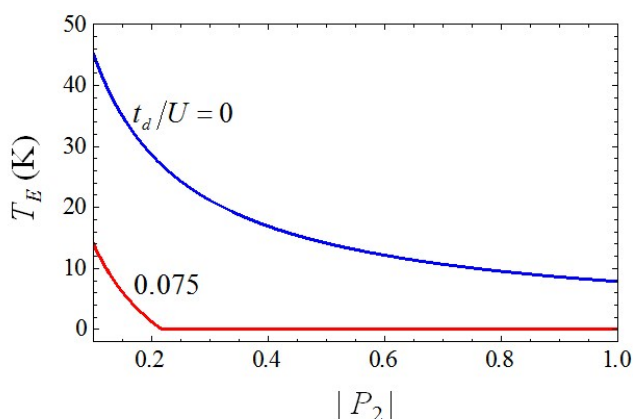
Figure 9. Critical temperature of entanglement in the cell **1** calculated at two different values of t_d/U shown in the figure. The remaining parameters are the same as those in Figure 6.

An additional illustration of this statement is provided by Fig. 9 in which the critical temperature T_E is shown as function of $|P_2|$ which varies in the range $0.1 \leq |P_2| \leq 1$. For both considered values of parameters t_d/U and for $t_d/U = 0$ the temperature T_E decreases with the increase of $|P_2|$, but for $t_d/U = 0.075$ it vanishes at the critical value of $|P_2|$ at which the

ground state changes the spin from $S = 0$ to $S = 1$, while providing $t_d/U = 0$ the temperature T_E slowly goes down with the increase of $|P_2|$ and reaches a finite value $\approx 9K$ at $|P_2|=1$.

4. Influence of the electron transfer and vibronic coupling on quantum entanglement

As far as the model is based on the parametric Hamiltonian it seems to be reasonable to reveal the effects of different parameters involved in the model on the main characteristics of the entanglement. First, let us examine the influence of the transfer parameter t_n^2/U on the effective exchange J_{eff}. For small values of $4t_n^2/U$ the electron deloclization in the spin-singlet states is not too pronounced and so the low-lying levels belonging to $S = 1$ and $S = 0$ manifolds are stabilized almost equally under the action of the input cell. As a result the singlet-triplet gap proves to be almost unaffected by P_2 (Fig. 10a). For this reason the critical temperature and the entanglement are only weakly dependent on P_2 and, as a consequence,

(a)   (b)
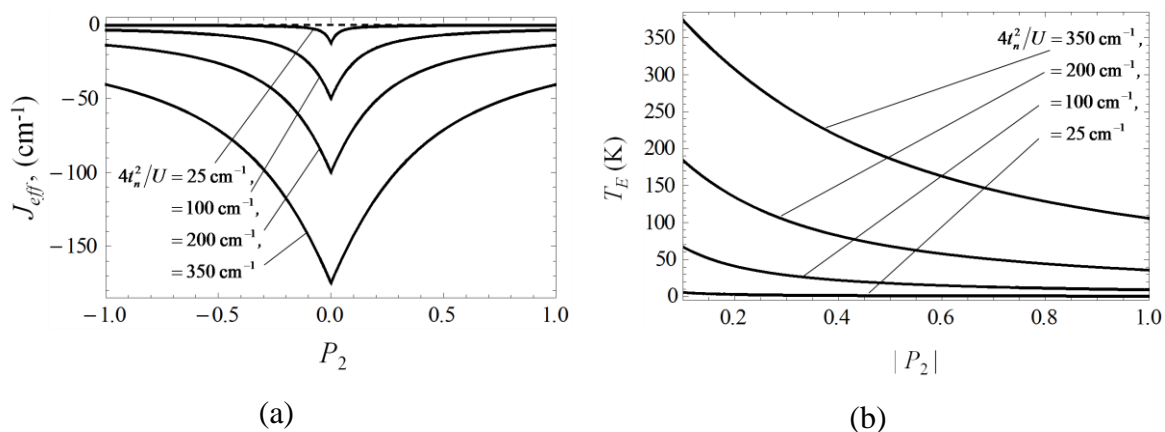
Figure 10. Effect of the parameter $4t_n^2/U$ on the effective exchange coupling $J_{eff}\left(P_2\right)$ (a) and on the dependences $T_E\left(P_2\right)$ (b): $t_d/U = 0$, $\upsilon = 0$, the values of $4t_n^2/U$ are indicated in the plots. The distances b and c are the same as in Figure 6.

the external field control of the entanglement in this case is hindered. This is clearly seen from Fig. 10b related to the case of vanishing diagonal transfer (the inclusion of the non-zero diagonal transfer does not change this general conclusion). Additionally, for small $4t_n^2/U$ -values the singlet-triplet gap is also small and hence the temperature T_E proves to be very low.

Effect of the vibronic coupling is illustrated by Figures 11 and 12. When the vibronic coupling is strong enough it significantly suppresses the electron delocalization in the spin-

(a)   (b)
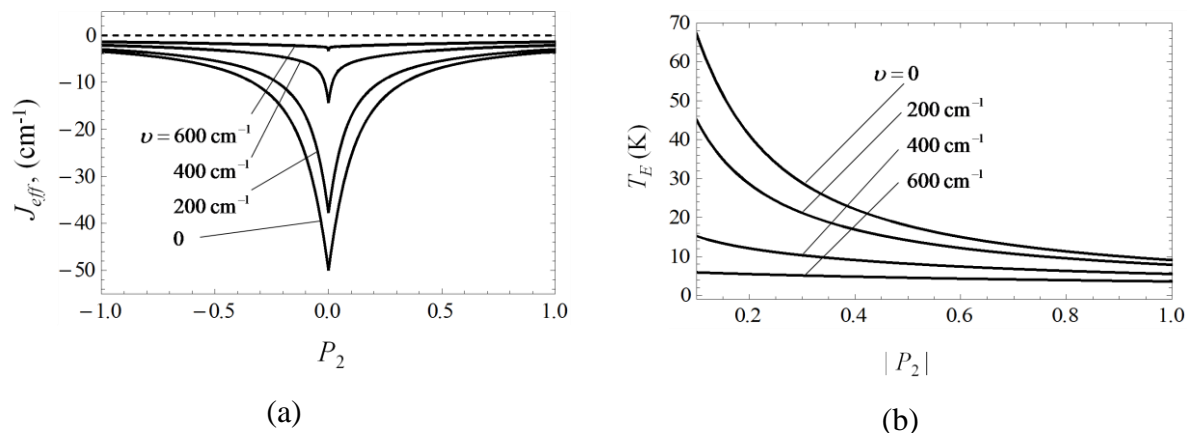
Figure 11. Effect of the parameter υ on the dependences $J_{eff}(P_2)$ (a) and $T_E(P_2)$ (b) calculated with $t_d/U = 0$. The values of υ are indicated in the plots, the remaining parameters are the same as those in Fig. 6.

singlet states making them more similar to the spin-triplet states which do not exhibit any electron delocalization in the strong-U approximation. Due to that in the case of strong vibronic coupling the action of the input cell almost equally stabilizes the low lying levels of $S=1$ and $S=0$ sets, that means that the singlet-triplet gap is almost independent on polarization

(a)   (b)
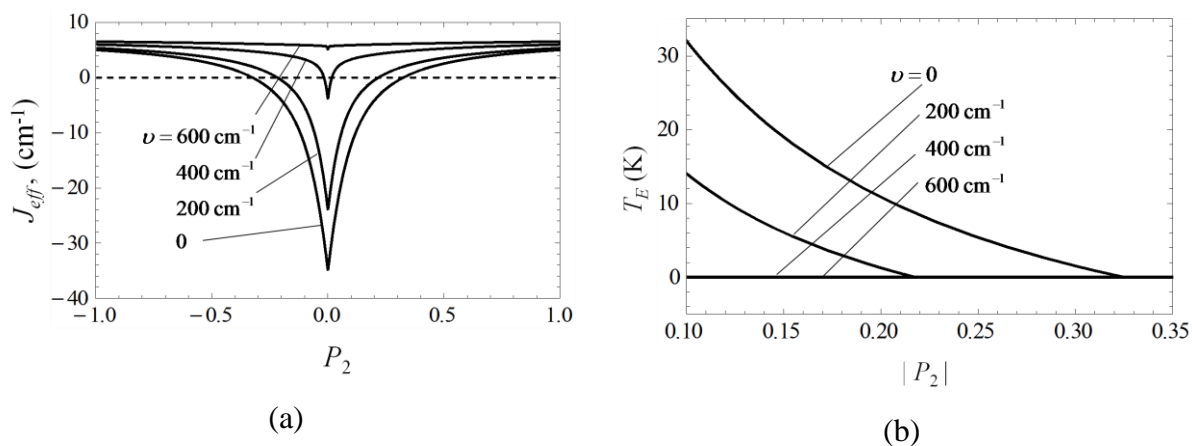
Figure 12. Effect of the parameter υ on the dependences $J_{eff}(P_2)$ (a) and $T_E(P_2)$ (b) calculated with $t_d/U = 0.075$. The values of υ are indicated in the plots, the remaining parameters are the same as those in Fig. 6.

P_2. For this reason, the critical temperature and the entanglement are weakly dependent on P_2 in the limit of strong vibronic coupling. This observation is common for the both considered cases $t_d = 0$ and $t_d \neq 0$ ($t_d/U = 0$ and $t_d/U = 0.075$ in Figures 11 and 12), although the t_d transfer leads to remarkable qualitative effects which are visible when comparing Figures 12 and 13. Thus providing $t_d/U = 0.075$ and strong vibronic coupling the spin-triplet is the ground state in the isolated cell (i.e. when P_2=0). The action of the input cell ($P_2 \neq 0$) results in the additional stabilization of the S=1 level and, thus, the entanglement does not occur at any values of P_2. Providing moderate vibronic coupling the spin-singlet is the low lying level, and just in this case the input cell is able to change the ground spin level under the action of the input cell. The spin-crossover occurs at some critical value of $|P_2|$, which increases with the decrease of the vibronic coupling, so that when the spin-triplet becomes the ground state the entanglement disappears.

5. Summary

We have considered a tetrameric MV units accommodating electronic pair which play role of cells in molecular QCA. The theoretical model includes the key interactions which act in an isolated MV cell (output cell), namely, the electrostatic interaction between the electrons, electron transfer and vibronic interaction. It is assumed that the input cell produces the electrostatic field which acts on the output cell. As in earlier papers it is supposed that the Coulomb interaction between instantly localized electrons within the cell is strong enough to localize the electronic pair in antipodal positions. Under this condition, as well as due to the vibronic localization of the electronic pair, the cell can encode the binary information which is controlled by the neighboring cells. We show that under certain conditions the low lying spin-vibronic levels of the cell affected by the field of the neighboring cell can be regarded as originating from an effective Heisenberg-type spin-spin interaction with the effective exchange parameter being dependent on the polarization of the neighboring cell. This physical situation is favorable for the observation of the controllable quantum entanglement of the two electrons in the output cell whose characteristics are closely related to the sign and strength of such spin-spin interaction [20].

The effective spin-spin coupling is shown to depend on the internal parameters of the cell (transfer parameters, vibronic coupling) as well as on the degree of the induced polarization. Within a simplified two-level picture of the low lying vibronic levels we evaluate the quantum entanglement system represented by the two electrons in the cell and show how the entanglement and concurrence can be controlled in a voluntary manner via the polarization

of the neighboring cell and temperature. The influence of the electron transfer (in particular, transfer pathways) and vibronic coupling on the quantum entanglement was examined in detail. A possibility to control the entanglement by the applied electric field has been proposed [51]. Since the Coulomb interaction of the neighboring cells in QCA schemes is, in general, strong, one can expect that the influence of the field can be much enhanced. Overall, a possible existence and, especially, control of the entanglement in the molecular MV cells of QCA opens new perspectives in molecular spintronics and information technologies. Finally, it is to be noted that the present study is focused on the molecular problem, so that the remaining question related to the properties of the systems under consideration in solid state or/and on the surface remains open. We hope to consider in future the problem of relaxation (peculiar to solids) and behavior of the cells on the surface.

Acknowledgment

References

1. M.A. Nielsen, I.L. Chuang, *Quantum Computation and Quantum Information*, Cambridge Univ. Press, Cambridge, 2000.

2. R. Vathsan , *Introduction to Quantum Physics and Information Processing*, CRC Press, Taylor & Francis Group, 2016.

3. *The Physics of Quantum Information: Quantum Cryptography, Quantum Teleportation and Quantum Computation*, Eds.: D. Bouwmeester, A. Ekert, A. Zeilinger, Springer, Berlin, 2000.

4. A.A. Kokin, *Solid State Quantum Computers on Nuclear Spins*, Computer Science Institute, Russian Academy of Sciences, Moscow, 2004 (in Russian).

6. K.A. Valiev, Quantum computers and quantum computations, *Usp. Fiz. Nauk* , 2005, **175** (1), 3-39 [*Phys.-Usp.,* 2005, **48** (1), 1-36].

7. P.G. Kwiat, K. Mattle, H. Weinfurter, A. Zeilinger, New high-intensity source of polarization-entangled photon pairs, *Phys. Rev. Lett,* 1995, **75**, 4337–4341.

8. Z. Zhao, Y.-A. Chen, A.-N. Zhang, T. Yang, H. J. Briege, J.-W. Pan, Experimental demonstration of five-photon entanglement and open-destination teleportation*, Nature,* 2004, **430**, 54-58.

9. M . Arndt, O. Nairz, J. Vos-Andreae, C. Keller, G. van der Zouw, A. Zeilinger, Wave–particle duality of C_{60} molecules*, Nature*, 1999, **401**, 680–682.

10. A. Bencini, D. Gatteschi, *EPR of Exchange Coupled Systems*, Dover, Mineola, NY, 2012.

11. D. Gatteschi, R. Sessoli, J. Villain, *Molecular Nanomagnets*, Oxford University Press, 2006.

12. C. Benelli, D. Gatteschi, *Introduction to Molecular Magnetism, From Transition Metals to Lantanides*, Willey-VCH, Chennai, Singapore, 2015.

13. *Molecular Cluster Magnets*, Ed.: R.E.P Winpenny, World Scientific Series in Nanoscience, Vol. 3, 2011.

14. M.N. Leuenberger, D. Loss, Quantum computing in molecular magnets, *Nature* , 2001, **410**, 789-793.

15. F. Meier, J. Levy, D. Loss, Quantum computing with antiferromagnetic spin clusters, *Phys. Rev*. B, **68**, 134417-134432, 2003.

16. F. Troiani, A. Ghirri, M. Affronte, S. Carretta, P. Santini, G.Amoretti, S. Piligkos, G. Timco, R. E. P. Winpenny, Molecular Engineering of Antiferromagnetic Rings for Quantum Computation*, Phys. Rev. Lett*., 2005, **94**, 207208-4.

17. M. Affronte, I. Casson, M. Evangelisti, A. Candini, S. Carretta, C. A. Muryn, S. J. Teat, J. Timco, W. Wersndorfer, and R. E. P. Winpenny, Linking rings through diamines and clusters: Exploring synthetic methods for making magnetic quantum gates, *Angew. Chem., Int. Ed*., 2005, **44**, 6496-6500.

18. W. Wersndorfer, Molecular Magnets: A long-lasting phase , *Nat. Mater.* 2007, **6**, 174-176,

19. S. Carretta, P. Santini, G. Amoretti, F. Troiani, M. Affronte, Spin triangles as optimal units for molecule-based quantum gates *Phys. Rev. B*, 2007, **76**, 024408-5.

20. S. M. Aldoshin, E.B. Feldman, M. A. Yurishchev, Quantum Entanglement in Nitrosyl Iron Complexes,   *J. Exp. Theor. Physics,* 2008, **107**, 804–811.

21. G.A. Timco, S. Carretta, F. Troiani, F. Tuna, R. J. Pritchard, C.A. Muryn, E. J. L. McInnes, A. Ghirri, A. Candini, P. Santini, G. Amoretti, M. Affronte, R.E.P. Winpenny, Engineering the coupling between molecular spin qubits by coordination chemistry, *Nature Nanotechnology* , 2009, **4***, 173-178.

22. A. Candini, G. Lorusso, F. Troiani, A. Ghirri, S. Carretta, P. Santini, G. Amoretti, C. Muryn, F. Tuna, G. Timco, E.J.L. McInnes, R.E.P. Winpenny, W. Wernsdorfer,

M. Affronte, Entanglement in supramolecular spin systems of two weakly coupled antiferromagnetic rings (Purple-Cr$_7$Ni), *Phys. Rev. Lett.,* 2010, **104**, 037203-4.

23. F. Luis, A. Repollés, M. J. Martínez-Pérez, D. Aguilà, O. Roubeau, D. Zueco, P. J. Alonso, M. Evangelisti, A. Camón, J. Sesé, L. A. Barrios, G. Aromí, Molecular prototypes for spin-based CNOT and SWAP quantum gates, *Phys. Rev. Lett.,* 2011, **107**, 117203-4.

24. D. Aguilà, L. A. Barrios, V. Velasco, O. Roubeau, A. Repollés, P. J. Alonso, J. Sesé, S. J. Teat, F. Luis, G. Aromí, Heterodimetallic [LnLn′] Lanthanide complexes: toward a chemical design of two-qubit molecular spin quantum gates, *J. Am. Chem. Soc*. 2014, **136**, 14215−14222.

25. J. F. Soria, E. M. Pineda, A. Chiesa, A. Fernandez, S. A. Magee, S. Carretta, P. Santini, I. J. V. Yrezabal, F. Tuna, G.A. Timco, E. J.L. McInnes, R. E.P. Winpenny A modular design of molecular qubits to implement universal quantum gates *Nature Communications* 7, Article number: 11377 (2016) doi:10.1038/ncomms11377.

26. F. Dolde, I. Jakobi, B. Naydenov, N. Zhao, S. Pezzagna, C. Trautmann, J. Meijer, P. Neumann, F. Jelezko, J. Wrachtrup, Room-temperature entanglement between single defect spins in diamond, *Nature Physics,* 2013*,* **9**,139–143.

27. S.M. Aldoshin, E. B. Fel'dman, M.A. Yurishchev, Quantum entanglement and quantum discord in magnetoactive materials, *Low Temp. Phys*., 2014, **40** (1), 3-16.

28. C.S. Lent, P. Tougaw, W. Porod, G. Bernstein, Quantum cellular automata, *Nanotechnology,* 1993, **4**, 49-57.

29. W. Porod, C.S. Lent , G.H. Bernstein, A.O. Orlov, I. Amlani , G.L. Snider , J.L. Merz, Quantum-dot cellular automata: computing with coupled quantum dot , *Int. J. Electronics*, 1999, **86**, 549-590.

30. P. D. Tougaw, C.S. Lent, *J. Appl. Phys*.,Logical devices implemented using quantum cellular automata, 1994, **75,** 1818-1825.

31. C.S. Lent, *Science*, Bypassing the transistor paradigm, 2000, **288**, 1597-1599.

32. C.S. Lent, B. Isaksen, M. Lieberman, *J. Am. Chem. Soc*., Molecular quantum-dot cellular automata, 2003, **125**, 1056-1063.

33. M. Lieberman, S. Chellamma, B. Varughese, Y. Wang, C. Lent, G.H. Bernstein, G. Snider, F.C. Peiris*,* Quantum-dot cellular automata at molecular scale, *Ann. N.Y. Acad. Sci*. 2002, **960**, 225-239.

34. C.S. Lent, P. D. Tougaw, Lines of interacting quantum-dot cells: A binary wire, *J. Appl. Phys*. 1993, **74**, 6227-6233.

35. X. Wang, J. Ma, *Phys. Chem. Chem. Phys.* Electron switch in the double-cage fluorinated fullerene anions, $e^-@C_{20}F_{18}(XH)_2C_{20}F_{18}$ (X = N, B): new candidates for molecular quantum-dot cellular automata 2011, 13, 16134-16137.

36. B. Schneider, S. Demeshko, S. Neudeck, S. Dechert, F. Meyer, Mixed-Spin $[2\times2]$ Fe_4 grid complex optimized for quantum cellular automata, *Inorg. Chem.* 2013, **52**, 13230-13237.

37. Y. Lu, C.S. Lent, Counterion-free molecular quantum-dot cellular automata using mixed valence zwitterions- a double-dot derivative of the [*closo*-1- $CB_9H_{10}]^-$ cluster *Chem. Phys. Lett.* 2013, **582**, 86-89.

38. J. Jiao, G.J. Long, L. Rebbouh, F. Grandjean, A.M. Beatty, T.P. Fehlner, Properties of a mixed-valence $(Fe^{II})_2(Fe^{III})_2$ square cell for utilization in the quantum cellular automata paradigm for molecular electronics, *J. Am. Chem. Soc.* 2005, **127**, 17819-17831.

39. R.C. Quardokus, Y. Lu, N.A. Wasio, C.S. Lent, F. Justaud, C. Lapinte, S.A. Kandel, Through-bond versus through-space coupling in mixed-valence molecules: observation of electron localization at the single-molecule scale *J. Am. Chem. Soc.*, 2012, **134**, 1710-1714.

40. H. Qi, S. Sharma, Z. Li, G. L. Snider, A.O. Orlov, C.S. Lent, T.P. Fehlner, Molecular quantum cellular automata cells. Electric field driven switching of a silicon surface bound array of vertically oriented two-dot molecular quantum cellular automata, *J. Am. Chem. Soc.*, 2003, **125**, 15250-15259 .

41. H. Qi, A. Gupta, B. C. Noll, G.L. Snider, Y. Lu, C. Lent, T. P. Fehlner, Dependence of field switched ordered arrays of dinuclear mixed-valence complexes on the distance between the redox centers and the size of the counterions, *J. Am. Chem. Soc.,* 2005, **127**, 15218-15227.

42. Z. Wei, S. Guo, S.A. Kandel, Observation of Single Dinuclear Metal-Complex Molecules Using Scanning Tunneling Microscopy, *J. Phys. Chem. B*, 2006, **110**, 21846-21849.

43. S. Guo, S.A. Kandel, Scanning Tunneling Microscopy of Mixed Valence Dinuclear Organometallic Cations and Counterions on Au(111) ,*J. Phys. Chem. Lett.* 2010, 1, 420-424.

44. N.A. Wasio,. RC. Quardokus, R.P. Forrest, S.A. Corrcelli, Y. Lu, C.S. Lent, F. Justaud, C. Lapinte, S.A. Kandel, STM Imaging of Three-Metal-Center Molecules: Comparison of Experiment and Theory For Two Mixed-Valence Oxidation States, *J. Phys. Chem.C*, 2012, 116, 25486-25492.

45. S.B. Braun-Sand, O. Wiest, Biasing Mixed-Valence Transition Metal Complexes in Search of Bistable Complexes for Molecular Computing, *J. Phys. Chem. A,* 2003, **107**, 285-291.

46. B. Tsukerblat, A. Palii, J.M. Clemente-Juan, Self-trapping of charge polarized states in four dot molecular quantum cellular automata: bi-electronic tetrameric mixed-valence species, *Pure & Applied Chemistry*, 2015, **87(3)**, 271-282.

47. B. Tsukerblat, A. Palii, J.M. Clemente-Juan, E. Coronado, Mixed-valence, molecular four-dot unit for quantum cellular automata: vibronic self-trapping and cell-cell response, *J. Chem. Physics,* 2015, **143**, 134307-15.

48. S.B. Piepho, E.R.Krausz, P.N. Shatz, Vibronic coupling model for calculation of mixed valence absorption profiles, *J. Am. Chem. Soc.* 1978**, 100**, 2996-3005.

49. S. Hill, W.K. Wootters, Entanglement of a pair of quantum bits. *Phys. Rev. Lett.* 1997, **78**, 5022-5026.

50. W. K. Wootters, Entanglement of formation of an arbitrary state of two qubits, *Phys. Rev. Lett.*,1998, **80,** 2245-2249.

51. O. O. Brovko, O. V. Farberovich, V. S. Stepanyuk, Electric field for tuning quantum entanglement in supported clusters, *J. Phys.: Cond. Matter*, 2014, **26,** 315010-4.